Title

Mode Analysis of Phase-Constant Nonreciprocity in Ferrite-Embedded CRLH Metamaterials

Journal

IEICE TRANSACTIONS ON ELECTRONICS, E96C(10)

ISSN

1745-1353

Authors

Porokhnyuk, Andrey
Ueda, Tetsuya
Kado, Yuichi
et al.

Publication Date

2013

DOI

10.1587/transele.E96.C.1263

Peer reviewed

PAPER Special Section on Emerging Technologies and Applications for Microwave and Millimeter-Wave Systems

Mode Analysis of Phase-Constant Nonreciprocity in Ferrite-Embedded CRLH Metamaterials

Andrey POROKHNYUK[†a)], ***Nonmember***, **Tetsuya UEDA**[†], **Yuichi KADO**[†], ***and*** **Tatsuo ITOH**[††], ***Members***

SUMMARY Phase-nonreciprocal ε-negative and CRLH metamaterials are analyzed using a new approach in which field analysis and transmission line model are combined. The examined one-dimensional nonreciprocal metamaterials are composed of a ferrite-embedded microstrip line periodically loaded with shunt stubs. In the present approach, the phase constant nonreciprocity is analytically estimated and formulated under the assumption of operating frequency far above the ferromagnetic resonant frequency. The present approach gives a good explanation to the phenomenon in terms of ferromagnetic properties of the ferrite and asymmetric geometry of the metamaterial structure, showing a good agreement with numerical simulations and experiment.

key words: *metamaterials, leaky-wave antennas, electromagnetic analysis, transmission line matrix methods, beam steering, ferrite devices*

1. Introduction

In the field of metamaterial-based functional device electronics that emerged in the latest decade, a great attention has been paid to reciprocal composite right/left handed (CRLH) metamaterials [1]–[4]. In combination of the CRLH metamaterials and nonreciprocal device technology, nonreciprocal transmission line-based metamaterials were proposed. In the early work, they are generally considered in view of nonreciprocity in the amplitude of transmission coefficients caused by dominance of CRLH modes in one direction and damping modes in the opposite direction of transmission for the applications to isolators and circulators [5]–[8].

From a phase-controlling point of view, phase-nonreciprocal CRLH metamaterial have been proposed and demonstrated [9], [10]. They can support right-handed (RH) mode propagation with positive effective refractive index in one direction and left-handed (LH) mode propagation with negative refractive index in the opposite direction of power transmission at the same frequency, resulting in unidirectional phase flow [9]. This phenomenon was applied to the design of nonreciprocal leaky wave antennas with enhanced gain and directivity by recycling some part of propagating waves reflected at the terminal [10], [11], as well as to pseudo-traveling-wave resonator [10], [12], [13] that is similar to zeroth-order resonator [1], [3], [14], [15] in that the resonant frequency is independent of the size, but has unique field profile with uniform magnitude and linear phase gradient along the structure. The pseudo-traveling-wave resonator with tunable phase gradient by varying the applied dc magnetic field was implemented for beam scanning antennas [10], [13], [16].

In our previous approach, when estimating phase nonreciprocal transmission characteristics of the CRLH metamaterials, an equivalent circuit model was employed in which nonreciprocal transmission line sections with different phase constants depending on propagation directions were introduced into the conventional CRLH transmission line model [9]. However, the phase nonreciprocity in the nonreciprocal sections was numerically extracted from separate full-wave electromagnetic simulation results. The different popular method for analyzing reciprocal and nonreciprocal periodic structures using transmission matrix technique was described in [17], [18]. But it was not applied to ferrite-based left-handed metamaterials previously. Likewise, dominant electromagnetic modes in the structures were not analyzed using this method.

In order to avoid relying on numerical simulation, we proposed recently a new approach to combine a simplified field analysis and transmission line model for the ε-negative metamaterial [19], expanding the method described above [18]. However, the application of the approach was limited to a specific ε-negative structure in lossless case and the nonreciprocity in phase constant had neither been intrinsically formulated nor discussed from a physical point of view.

In this paper, we show the detailed procedure in the proposed approach using a simplified field theory and transmission line model to analyze phase-nonreciprocal metamaterials. The periodic section is decomposed into several sections in the longitudinal direction. Generalized nonreciprocal dispersion relation is derived and the eigenmode solution for each section is achieved. The phase-constant nonreciprocity of the ε-negative metamaterial structure is approximately formulated and estimated under the assumption of operating frequency far above the ferromagnetic resonant frequency. It gives a good explanation to the phenomenon and is expressed explicitly in terms of ferromagnetic properties of the ferrite and asymmetric geometry of the metamaterial structure, showing a good agreement with numerical simulations and experiment. The applicability of the approach to nonreciprocal and CRLH structures is also discussed and proven by simulation.

Manuscript received February 15, 2013.
Manuscript revised May 25, 2013.

[†]The authors are with the Department of Electronics, Kyoto Institute of Technology, Kyoto-shi, 606-8585 Japan.
[††]The author is with the Department of Electrical Engineering, University of California at Los Angeles, Los Angeles, CA 90095, USA.
a) E-mail: d1821008@edu.kit.ac.jp

DOI: 10.1587/transele.E96.C.1263

2. Nonreciprocal Edge-Guided Modes

The phase constant-nonreciprocal metamaterial under consideration is shown in Fig. 1. It is composed of a microstrip line with a ferrite rod embedded under the center strip and occupying all the space beneath it. An internal dc magnetic field H_o and induced saturation magnetization M_S in the ferrite rod are directed normal to the microstrip surface. The microstrip line is periodically loaded with microstrip stubs, as shown in Fig. 1. The stubs play two important roles in providing negative effective permittivity in the cutoff band and in introducing an asymmetry of the wave-guiding structure with respect to a plane including the saturation magnetization vector and the longitudinal direction.

It is well-known that the quasi-TE edge-guided modes [20] are dominant along the normally magnetized ferrite microstrip line. The waves propagate in opposite directions along opposite side walls below the strip edge, which is depicted in Fig. 1 and Fig. 2 with red- and blue-filled profiles of the field component E_z as a function of x. If the structure is symmetric, the transmission is reciprocal. Otherwise with introduction of the asymmetry, the transmission shows nonreciprocal characteristics. Similar transmission characteristics were also confirmed in ferrite rod-embedded microstrip lines [21], [22]. In our approach, the asymmetry of the structure is described and approximated with different boundary conditions on the side walls of the ferrite-rod embedded microstrip line [19]. Periodic insertion of load stubs provides such a difference of boundary conditions and induces nonreciprocity in discrete and partial domains along the microstrip line. In order to analyze a dominant mode along the structure using field theory, the structure is decomposed into two different types of uniform sections, as shown in Fig. 1(b). One section is a reciprocal section (RS), in which no stubs are inserted and the structure is symmetric. The other section is a nonreciprocal section (NRS) in which an inserted microstrip stub provides asymmetry of boundary conditions on the side walls of the rod. These asymmetric boundary conditions are described by boundary admittances that are ratios of magnetic to electric field components on the plane of side walls $Y_1 = H_y/E_z$ at $x = 0$ and $Y_2 = -H_y/E_z$ at $x = w$ as outlined in Fig. 2 with dashed lines. In the reciprocal section without load stubs, both side walls correspond to a magnetic wall. In the nonreciprocal section, the microstrip stub provides imaginary input impedance that is converted to boundary admittance Y_2 on the corresponding side wall [19]. It is convenient to treat the microstrip stub as a simple transformer of terminating impedance. The input impedance of the shunt stub has a positive imaginary value when the stub length is less than quarter wavelength. It should be mentioned that introduction of different stubs on both sides can give several potential advantages, such as enhancement of the phase-constant nonreciprocity or additional control of nonreciprocal dispersion.

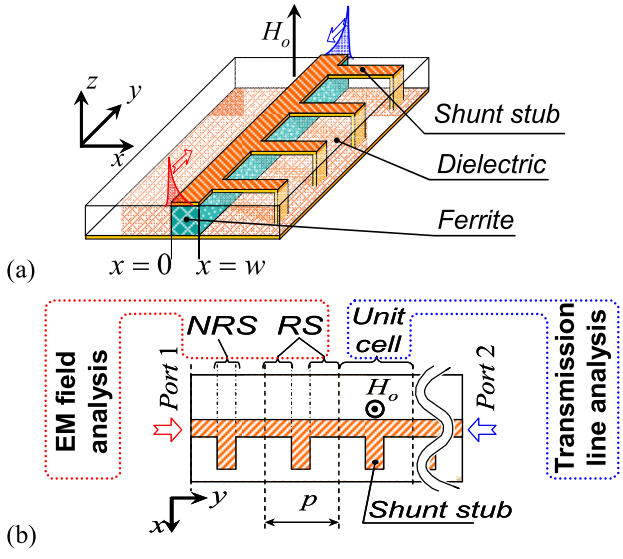

Fig. 1 Transmission line based ε-negative metamaterial structure. (a) Schematic appearance. (b) Combined field theory and transmission line analysis model.

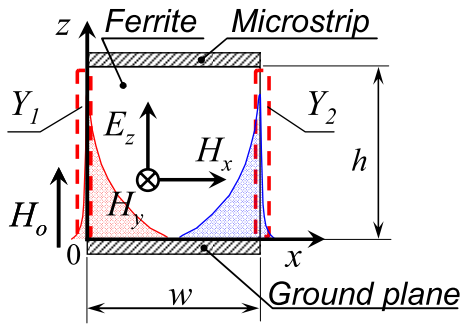

Fig. 2 Electromagnetic model of ferrite rod-embedded microstrip line in cross-section.

3. Eigen-Mode Analysis in Reciprocal and Nonreciprocal Sections

3.1 Simplified Electromagnetic Model

In the present approach, the dominant electromagnetic waves propagating along the ferrite-embedded microstrip line are simplified to TE modes. The analysis is done under the assumption of the substrate thickness to be much smaller than the wavelength. The ferrite rod is also treated as homogenous and uniformly saturated by the dc magnetic field H_o. Such assumptions greatly simplify the problem and virtually give a uniform field distribution along z-axis. Eigenmode analysis is applied separately to reciprocal and nonreciprocal sections, as shown in Fig. 2. The analysis is performed only in cross-section of the ferrite rod between left and right boundary walls. In the reciprocal section, admittances Y_1 and Y_2 imposed on the left and right walls are zero for magnetic wall boundaries. In the nonreciprocal section, the left wall where no stub is inserted, has $Y_1 = 0$ for magnetic wall. The admittance Y_2 takes finite imaginary

value on the right wall where the stub is inserted.

We begin with a simple Helmholtz wave equation to find the nonreciprocal eigenmode solution,

$$\frac{\partial^2 E_z}{\partial x^2} + k_x^2 E_z = 0 \tag{1}$$

with

$$k_x^2 = \mu_e \varepsilon_r \left(\frac{\omega}{c}\right)^2 + \gamma^2, \quad \mu_e = (\mu^2 - \mu_a^2)/\mu$$

where k_x describes transverse wave number component along x-axis, and $\gamma = \alpha + j\beta$ is propagation constant in the longitudinal y-direction. The quantities α and β are attenuation and phase constants, respectively. The quantity ε_r is dielectric constant of the ferrite, while μ and μ_a denote conventional diagonal and off-diagonal components of Polder's tensor $\hat{\mu}_r$ for the ferrite media magnetized along z-axis.

$$\hat{\mu}_r = \begin{bmatrix} \mu & j\mu_a & 0 \\ -j\mu_a & \mu & 0 \\ 0 & 0 & 1 \end{bmatrix}, \quad \begin{matrix} \mu = 1 + \dfrac{\omega_H \omega_M}{\omega_H^2 - \omega^2}, & \mu_a = \dfrac{\omega_M \omega}{\omega_H^2 - \omega^2}, \\ \omega_H = |g|\mu_o H_o, & \omega_M = |g|\mu_o M_S \end{matrix} \tag{2}$$

where ω is an operational frequency, μ_o is the permeability of vacuum, and g is the gyromagnetic ratio.

3.2 Dispersion Relations

The eigenmode analysis of (1) with applied boundary conditions described by Y_1 and Y_2 gives generalized dispersion relations in reciprocal and nonreciprocal sections,

$$\Phi = j\cot(wk_x) - \frac{\dfrac{\gamma^2}{(\omega/c)} + \left(\dfrac{\omega}{c}\right)\mu(\tilde{Y}_1\tilde{Y}_2\mu_e + \varepsilon_r)}{\mu k_x(\tilde{Y}_1 + \tilde{Y}_2)} - \frac{\gamma\mu_a(\tilde{Y}_1 - \tilde{Y}_2)}{\mu k_x(\tilde{Y}_1 + \tilde{Y}_2)} = 0 \tag{3}$$

with

$$\tilde{Y}_1 = Y_1\sqrt{\mu_o/\varepsilon_o}, \tilde{Y}_2 = Y_2\sqrt{\mu_o/\varepsilon_o}$$

where ε_o is the permittivity of vacuum. In (3), only the last term is an odd function of γ, thus determining nonreciprocity. Equation (3) can be simplified to dispersion relation for insertion with shunt stub only from one side with $\tilde{Y}_1 = 0$,

$$\cot(wk_x) = \frac{1}{j\tilde{Y}_2}\left(\frac{\gamma^2}{(\omega/c)k_x\mu} + \frac{\varepsilon_r(\omega/c)}{k_x}\right) + j\frac{\gamma\mu_a}{\mu k_x} \tag{4}$$

Equations (3) and (4) are transcendental and have no solution in algebraic form; neither series expansion gives a consistent solution. We used Newton method to find complex values of γ. However, in the reciprocal section without stubs, $Y_1 = Y_2 = 0$. Then, (3) reduces to $\gamma = \pm j(\omega/c)\sqrt{\mu\varepsilon_r}$ which is well-known edge-guided mode [20].

Figures 3(a) and (b) illustrate dispersion curves of reciprocal edge guided modes in reciprocal section and nonreciprocal modes in nonreciprocal section according to (4) for the lossless case. Red and blue colored lines represent

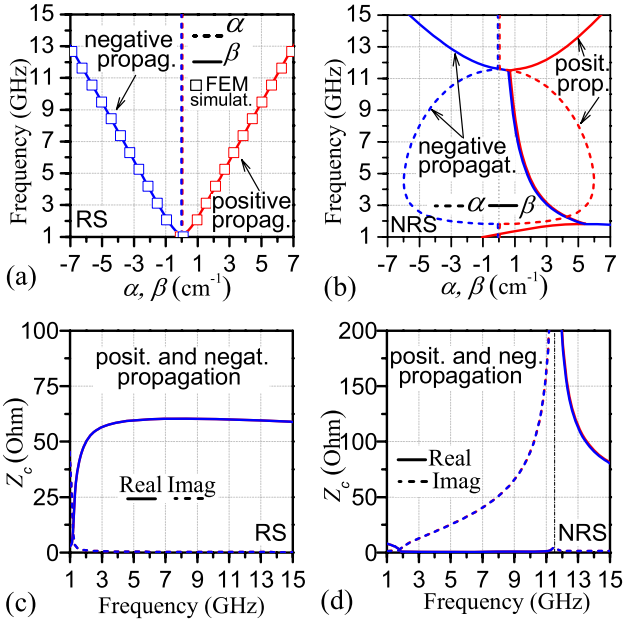

Fig. 3 Properties of RS and NRS. (a), (b) Dispersion characteristics. (c), (d) Characteristic impedances in both directions.

positive and negative transmission directions for α and β, including the sign. The configuration parameters used in the calculation are as follows; cross-section of the saturated ferrite rod is 0.8 mm × 0.8 mm, $\mu_o H_o$ = 10 mT and $\mu_o M_S$ = 175 mT. The right boundary admittance Y_2 was provided by input impedance of 1 mm-width and 2 mm-length shunt stub on dielectric substrate with dielectric constant of 2.6. The square marks in Fig. 3(a) represent the dispersion converted for convenience from the phase shift acquired with numerical simulation.

3.3 Estimate of Phase-Constant Nonreciprocity

In the previous section, we have derived generalized nonreciprocal dispersion relation (3) as eigenmode solution in the nonreciprocal section. Therefore, the phase-constant nonreciprocity can be estimated in an implicit manner by directly solving the transcendental equation. In order to understand the mechanism of nonreciprocity, it is more instructive and useful to explicitly express the phase-constant nonreciprocity in terms of the configuration parameters, such as magnetic properties of the ferrite and the asymmetry of the waveguide. In what follows, we will approximately formulate such information.

The nonreciprocal effects stem from the off-diagonal components in Polder's tensor (2), μ_a, in the ferrite medium. Before turning to nonreciprocal case, we find the eigenmode solution of (3) under the assumption $\mu_a = 0$ and find the solution for propagation constant $\gamma = \gamma_o$ that we call a zeroth-order approximation of γ. Taking into consideration nonreciprocal effects, we regard Φ in (3) as a function of μ_a and $\gamma = \gamma_o + \Delta\gamma_{NR}$, where $\Delta\gamma_{NR}$ is a magnitude of nonreciprocity induced by μ_a. In the vicinity of $\gamma = \gamma_o$ and $\mu_a = 0$, we can

express $\Delta\gamma_{NR}$ as

$$\Delta\gamma_{NR} = -\mu_a \frac{\partial}{\partial \mu_a} \Phi|_{\substack{\mu_a=0 \\ \gamma=\gamma_o}} \Big/ \frac{\partial}{\partial \gamma} \Phi|_{\substack{\mu_a=0 \\ \gamma=\gamma_o}}.$$

From (3) we achieve

$$\Delta\gamma_{NR} \approx \frac{\mu_a(\omega/c)(\tilde{Y}_1 - \tilde{Y}_2)}{\tilde{Y}_1\tilde{Y}_2\left(\frac{\omega}{c}\frac{\mu}{k_{xo}}\right)^2 - j\frac{\omega}{c}\frac{w\mu(\tilde{Y}_1+\tilde{Y}_2)}{\sin^2(wk_{xo})} - 1} \tag{5}$$

where a variable k_{xo} in (5) is defined by $k_{xo}^2 = \gamma_o^2 + \mu\varepsilon_r(\omega/c)^2$, and it can be approximately expressed from $\Phi|_{\mu_a=0,\gamma=\gamma_o} = 0$ using Taylor series by

$$k_{xo}^2 \approx \frac{j(\omega/c)\mu w\tilde{Y}_1\tilde{Y}_2 + \tilde{Y}_1 + \tilde{Y}_2}{\left(w^2\frac{(\tilde{Y}_1+\tilde{Y}_2)}{2} + \frac{w}{j(\omega/c)\mu}\right)}. \tag{6}$$

The expression (5) can be simplified under the assumption that the operation frequency is much higher than ω_H and ω_M. The nonreciprocity in propagation constant for generalized boundary condition is given by

$$\Delta\gamma_{NR} \approx j\frac{(\omega_M/c)(\tilde{Y}_2 - \tilde{Y}_1)}{w\left(\frac{\omega}{c}\right)\frac{(\tilde{Y}_2+\tilde{Y}_1)}{2} - 2j}. \tag{7}$$

The derivation of (7) is one of the main points of this work. For lossless cases when ω_M is real and $\tilde{Y}_1$, $\tilde{Y}_2$ are pure imaginary, $\Delta\gamma_{NR}$ is also pure imaginary, which implies that the nonreciprocity manifests itself only in the phase constant β as $\Delta\beta_{NR} = -j\Delta\gamma_{NR}$, that also comes into agreement with Fig. 3(b). For a specific structure with $\tilde{Y}_1 = 0$ in Fig. 1, (7) reduces to

$$\Delta\gamma_{NR}|_{\tilde{Y}_1=0} \approx j\frac{(\omega_M/c)}{\frac{w}{2}\left(\frac{\omega}{c}\right) + \frac{2}{j\tilde{Y}_2}}.$$

Equations (5) and (7) reveal the proportional dependence of the phase-constant nonreciprocity $\Delta\beta_{NR}$ on the saturation magnetization M_S. As it will be discussed in Sect. 4.3, (7) supports the experimental results in [13], in which the measured phase-constant nonreciprocity of the nonreciprocal CRLH transmission line was approximately proportional to the effective magnetization of the unsaturated ferrite. The nonreciprocity diminishes at higher frequencies with reduction of μ_a inversely proportional to ω. Equation (7) suggests that the use of ferrites with larger M_S can provide stronger nonreciprocity. It is also found from (7) that the phase-constant nonreciprocity is proportional to the factor $\tilde{Y}_1 - \tilde{Y}_2$, the difference of admittances at both side walls, which verify that the asymmetry of the waveguiding structure contributes to nonreciprocity. The factor $\tilde{Y}_1 + \tilde{Y}_2$ in the denominator of (5) or (7) shows total shunt admittance that can control the effective permittivity of the structure [23].

3.4 Characteristic Impedance

Characteristic impedances of each section are estimated from the field profiles as a ratio of integrals of the Poynting vector over the cross-section and surface current along the microstrip line,

$$Z_c = \frac{2P}{|I|^2} \approx \frac{h\int_0^w E_z H_x^* dx}{|\int_0^w H_x d\ x|^2} \tag{8}$$

Figures 3(c) and (d) illustrate the characteristic impedance obtained from (8) for reciprocal and nonreciprocal sections. It is found from the figure that in the absence of propagation losses, the characteristic impedance is reciprocal, regardless of phase constant nonreciprocity.

An important conclusion from Fig. 3(d) is that the nonreciprocal section supports ε-negative cutoff modes. This can be explained in terms of effective permeability and permittivity as

$$\varepsilon_{eff} = \mathrm{Re}\left(-\gamma\frac{j}{Z_c}\frac{c}{\omega}\frac{h}{w}\sqrt{\frac{\mu_o}{\varepsilon_o}}\right),$$
$$\mu_{eff} = \mathrm{Re}\left(\gamma\frac{Z_c}{j}\frac{c}{\omega}\frac{w}{h}\sqrt{\frac{\varepsilon_o}{\mu_o}}\right) \tag{9}$$

or below cutoff region,

$$\varepsilon_{eff} = \frac{-1}{\mathrm{Im}(Z_c)}\frac{\alpha}{(\omega/c)}\frac{h}{w}\sqrt{\frac{\mu_o}{\varepsilon_o}},$$
$$\mu_{eff} = \mathrm{Im}(Z_c)\frac{\alpha}{(\omega/c)}\frac{w}{h}\sqrt{\frac{\varepsilon_o}{\mu_o}} \tag{10}$$

In the cutoff region, the term $\alpha/(\omega/c)$ has positive value, and the imaginary part of the characteristic impedance $\mathrm{Im}(Z_c)$ is also positive. Therefore, (10) gives negative ε_{eff} and positive μ_{eff}.

3.5 Microstrip Stubs Model

As mentioned in the previous section, the sole role of inserted microstrip stubs in the proposed model is to provide boundary admittances Y_1 and Y_2 that are input admittances of the stubs normalized with respect to stub's effective cross-section. The input admittance can be altered via stub length and terminating conditions. The effective width of the stub should also be taken into account when defining a distance between neighboring stubs to avoid mutual coupling. In this paper, conventional relations describing properties of microstrip line were used to achieve input impedance of the shunt stubs [24]. The applicability of those relations was carefully examined using numerical FEM simulations.

3.6 Influence of Ferrite Losses on Dispersion

In the proposed model for the field analysis, we can easily take into account the magnetic and dielectric losses in the ferrite rod that introduce a considerable perturbation in γ. The magnetic losses are taken into account by replacing the ferromagnetic resonance frequency ω_H in the Gilbert form by $(\omega_H + j\omega\Delta H/H_o)$ [25]. The modification of Fig. 3(b) with the magnetic loss of $\mu_o\Delta H = 5$ mT is shown in Fig. 4. Real

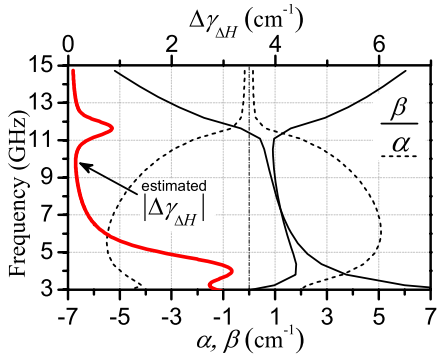

Fig. 4 Estimated perturbation of propagation constant $\Delta\gamma_{\Delta H}$, induced by magnetic dissipation with a factor $\mu_o \Delta H = 5$ mT.

parts of boundary admittances representing loss in the stubs are also taken into account, which provides slight smoothing of dispersion curves. The perturbation $\Delta\gamma_{\Delta H}$ of the propagation constant was plotted in Fig. 4 by applying perturbation theory to (3). The guided wave band and a frequency region just below the cutoff are less affected by magnetic dissipation, while the dispersion around cutoff is changed significantly due to slow group velocity.

4. Transmission Line Analysis of the Periodic Structure

4.1 ABCD Matrix Techniques

Circuit parameters in the nonreciprocal metamaterial structure, as shown in Fig. 5, are acquired from ABCD matrix of the simplest unit cell using transmission line analysis for infinitely periodic structure [17]. The unit cell is composed of two types of sections studied earlier, and its ABCD matrix F_{Cell} becomes a product of corresponding matrices for reciprocal section F_{RS} and for nonreciprocal section F_{NRS}

$$F_{Cell} = F_{RS} F_{NRS} F_{RS} = \begin{bmatrix} A_{Cell} & B_{Cell} \\ C_{Cell} & D_{Cell} \end{bmatrix}$$

Therefore, in the first place, it is necessary to determine the matrices of these sections. The matrix F_{RS} is a well known ABCD matrix of reciprocal transmission line [17]. On the other hand, the ABCD matrix F_{NRS} is derived in terms of different propagation constants γ^+ and γ^- in analogy to the transmission line section with nonreciprocal phase constants [9], where the indices "+" and "–" denote directions of transmission,

$$F_{NRS} = \begin{bmatrix} A_{NRS} & B_{NRS} \\ C_{NRS} & D_{NRS} \end{bmatrix} \tag{11}$$

with

$$A_{NRS} = e^{\Delta\gamma_{NR} l_N} \left(\cos(j\bar{\gamma}_N l_N) - j \frac{\Delta Z_N \sin(j\bar{\gamma}_N l_N)}{2\bar{Z}_N} \right)$$

$$B_{NRS} = -e^{\Delta\gamma_{NR} l_N} \left(j\bar{Z}_N \left(1 - \frac{\Delta Z_N^2}{4\bar{Z}_N^2} \right) \sin(j\gamma_N l_N) \right)$$

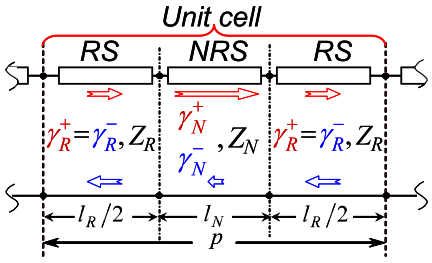

Fig. 5 Model of unit cell of the periodic metamaterial structure.

$$C_{NRS} = -e^{\Delta\gamma_{NR} l_N} \left(j \frac{\sin(j\gamma_N l_N)}{\bar{Z}_N} \right)$$

$$D_{NRS} = e^{\Delta\gamma_{NR} l_N} \left(\cos(j\gamma_N l_N) + j \frac{\Delta Z_N \sin(j\gamma_N l_N)}{2\bar{Z}_N} \right)$$

$$\bar{\gamma}_N = (\gamma^+ + \gamma^-)/2, \Delta Z_N = Z^+ - Z^-, \bar{Z}_N = (Z^+ + Z^-)/2$$

where Z^+ and Z^- are characteristic impedances in opposite directions, and l_N is a length of NRS. The magnitude of propagation-constant nonreciprocity in NRS is treated as $\Delta\gamma_{NR} = (\gamma^+ - \gamma^-)/2$. For lossless transmission line, characteristic impedance is reciprocal and $\Delta Z_N \approx 0$, as found in Fig. 3(d). In this case, (11) can be reduced to

$$F_{NRS} = e^{\Delta\gamma_{NR} l_N} \begin{bmatrix} \cos(j\bar{\gamma}_N l_N) & -j\bar{Z}_N \sin(j\bar{\gamma}_N l_N) \\ -j\frac{1}{\bar{Z}_N} \sin(j\bar{\gamma}_N l_N) & \cos(j\bar{\gamma}_N l_N) \end{bmatrix}$$

4.2 Dispersion and Bloch Characteristic Impedance

By applying periodic boundary conditions to the single unit cell in the longitudinal direction, we have

$$\begin{bmatrix} V_1 \\ I_1 \end{bmatrix} = F_{Cell} \begin{bmatrix} V_2 \\ I_2 \end{bmatrix} = \hat{I} e^{\gamma_{MM} p} \begin{bmatrix} V_2 \\ I_2 \end{bmatrix} \tag{12}$$

where V_i and I_i are voltages and currents at ports i ($i = 1, 2$) of the unit cell, and p is the period, γ_{MM} is the propagation constant in the whole periodic structure that will be treated in terms of attenuation and phase constants as $\gamma_{MM} = \alpha_{MM} + j\beta_{MM}$.

Eigenmode analysis of (12) allows deriving a dispersion relation for propagation constant γ_{MM} in the metamaterial,

$$\det(F_{Cell}) + e^{2\gamma_{MM} p} - e^{\gamma_{MM} p}(A_{cell} + D_{cell}) = 0. \tag{13}$$

For ε-negative structure, (13) becomes

$$\cosh(\gamma_{MM} p - \Delta\gamma_{NR} l_N) = \cos m_N \cos m_R + R^+ \sin m_N \sin m_R \tag{14}$$

with

$$R^+ = \frac{\Delta Z_N^2 - 4(\bar{Z}_N^2 + Z_R^2)}{8\bar{Z}_N \bar{Z}_R}, m_R = j\gamma_R l_R, m_N = j\bar{\gamma}_N l_N$$

where γ_R, l_R and Z_R are the propagation constant, length and characteristic impedance of reciprocal section, respectively. An example of dispersion curves obtained from (14) is illustrated in Fig. 6(a). The frequency characteristics of reciprocal and nonreciprocal sections are the same as in Fig. 3.

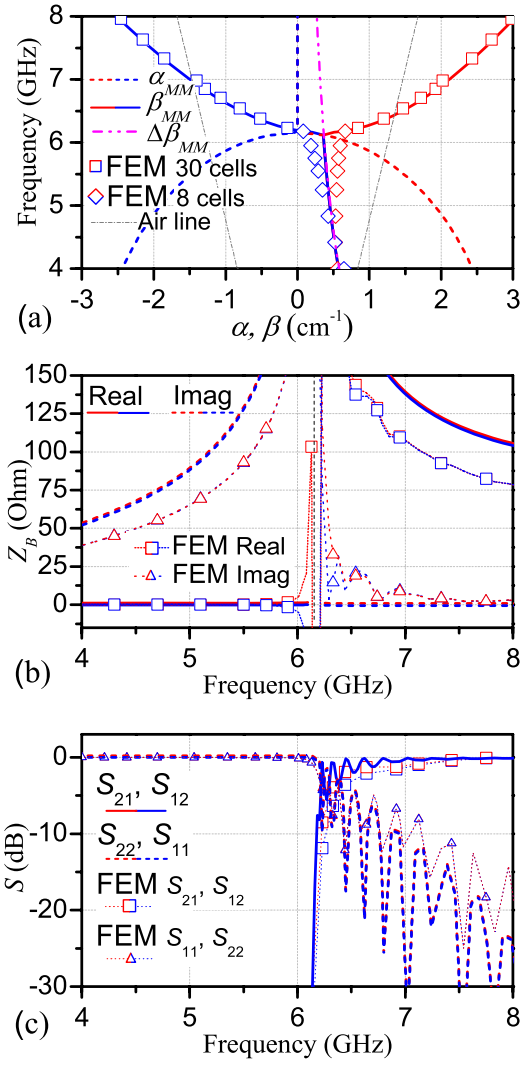

Fig. 6 Comparison of the proposed model with numerical simulation of the nonreciprocal ε-negative metamaterial. (a) Dispersion diagram. (b) Characteristic Bloch impedance. (c) S–parameters. Solid and dashed lines are for proposed approach, figure marks are for FEM simulation.

The calculations are made for lossless case with yttrium-iron garnet (YIG) rod of 0.8 mm × 0.8 mm in cross-section and 2 mm-length shunt-stubs inserted from one side of the structure. The internal dc field is $\mu_o H_o = 10$ mT. The values of l_R and l_N are 3 mm and 1 mm, respectively.

The Bloch impedance is derived by using voltage-current analysis in (12)

$$Z_B = \frac{2B_{Cell}}{D_{Cell} - A_{Cell} \pm \sqrt{(A_{Cell}+D_{Cell})^2 - 4e^{2\Delta\gamma_{NR} l_N}}}. \quad (15)$$

By substituting (11) into (15), Bloch impedance for ε-negative metamaterial is given by

$$Z_B = j\frac{Z_R\{\sin m_N(R^+ \cos m_R + R^-) - \sin m_R \cos m_N\}}{r \sin m_N \pm j\sqrt{1-(\cos m_N \cos m_R + R^+ \sin m_N \sin m_R)^2}} \quad (16)$$

with

$$R^- = \frac{\Delta Z_N^2 - 4(\bar{Z}_N^2 - Z_R^2)}{8\bar{Z}_N \bar{Z}_R}, \quad r = j\frac{\Delta Z_N}{2\bar{Z}_N}.$$

From (16), it is obvious that for lossless case, where $r \approx 0$, the Bloch impedance is always reciprocal, as it is illustrated in Fig. 6(b). We believe that notable discrepancy with numerical simulation in Fig. 6(b) is caused by the fringing effect of the microstrip line that is taken into account in the simulation and results in a little lower impedance values. However, we have not found a simple and accurate way of taking this into account in the current model because of the substrate nonuniformity.

Like the nonreciprocal section, the metamaterial structure should also be ε-negative. This can be proven by analyzing the imaginary part of Bloch impedance below the cutoff of nonreciprocal section. Supposing that the unit cell is much shorter than the wavelength, that gives $|m_N|, |m_R| \ll 1$, a low-order perturbation approximation can be applied to (16), reducing it with respect to positive propagation direction to

$$Z_B \approx \frac{Z_R(m_N(R^+ + R^-) - m_R)}{\sqrt{m_R^2 + m_N^2 - 2R^+ m_R m_N}} \approx \frac{-(Z_N m_N + Z_R m_R)}{\sqrt{m_R^2 + m_N^2 - 2R^+ m_R m_N}} \quad (17)$$

If we simplify R^+ and propagation constants using the lossless approximation as follows:

$$R^+ \approx \frac{j}{2}\left(\left|\frac{Z_R}{Z_N}\right| - \left|\frac{Z_N}{Z_R}\right|\right), \quad m_R \approx -\beta_R l_R, m_N \approx j\alpha_N l_N,$$

we can modify (17) further

$$Z_B \approx |Z_N| \sqrt{\left(\left|\frac{Z_R}{Z_N}\right| \beta_R l_R + \alpha_N l_N\right) \Big/ \left(\left|\frac{Z_N}{Z_R}\right| \beta_R l_R - \alpha_N l_N\right)}. \quad (18)$$

The relation (18) can give either positive real or positive imaginary values above and below the cutoff of the metamaterial structure respectively, where the cutoff is very roughly estimated by condition of $\beta_R l_R/|Z_R| = \alpha_N l_N/|Z_N|$. This characterizes the structure as ε-negative. Relation (18) gains a physical meaning if we rewrite it in terms of effective dielectric and magnetic constants ε_R, μ_R in reciprocal section and ε_N, μ_N in nonreciprocal section, respectively

$$Z_R = \sqrt{\frac{\mu_o \mu_R}{\varepsilon_o \varepsilon_R}}, |Z_N| = \sqrt{\frac{\mu_o \mu_N}{\varepsilon_o |\varepsilon_N|}}, \beta_R = \frac{\omega}{c}\sqrt{\varepsilon_R \mu_R}, \alpha_N = \frac{\omega}{c}\sqrt{|\varepsilon_N| \mu_N}, \varepsilon_N = -|\varepsilon_N|$$

$$Z_B \approx \sqrt{\frac{\mu_o}{\varepsilon_o}} \sqrt{\frac{(\mu_R l_R + \mu_N l_N)/p}{(\varepsilon_R l_R + \varepsilon_N l_N)/p}} = \sqrt{\frac{\mu_o}{\varepsilon_o}} \sqrt{\frac{\mu_{eff}}{\varepsilon_{eff}}}. \quad (19)$$

The upper term of (19) is proportional to effective permeability μ_{eff}, and the lower term is proportional to effective permittivity ε_{eff}, averaged along the longitudinal direction of the unit cell. The condition $\varepsilon_{eff} = (\varepsilon_R l_R + \varepsilon_N l_N)/p = 0$ determines the cutoff. The value of ε_N is explained in Sect. 3.4, while ε_R is a conventional effective permittivity of the microstrip line.

4.3 Magnitude of Phase-Constant Nonreciprocity

It is clearly seen from Fig. 6(a) that the dispersion diagram and particularly the magnitude of nonreciprocity is somewhat a result of combination of properties of nonreciprocal and reciprocal sections. It can be explained in lossless case by applying the perturbation theory to (14) with respect to parameter $\Delta\gamma_{NR}$ that induces a perturbation $\Delta\gamma_{MM}$ of propagation constant in the metamaterial as follows;

$$\Omega = \Omega|_{\substack{\Delta\gamma_{NR}=0\\ \Delta\gamma_{MM}=0}} + \Delta\gamma_{MM} \left.\frac{\partial\Omega}{\partial\Delta\gamma_{MM}}\right|_{\substack{\Delta\gamma_{NR}=0\\ \Delta\gamma_{MM}=0}} + \Delta\gamma_{NR} \left.\frac{\partial\Omega}{\partial\Delta\gamma_{NR}}\right|_{\substack{\Delta\gamma_{NR}=0\\ \Delta\gamma_{MM}=0}} = 0, \tag{20}$$

that is,

$$\Omega(\Delta\gamma_{NR}, \Delta\gamma_{MM}) = \cosh\left((\gamma_{MMo} + \Delta\gamma_{MM})p - \Delta\gamma_{NR} l_N\right) - \cos m_N \cos m_R - R^+ \sin m_N \sin m_R = 0$$

where $\Delta\gamma_{MMo}$ is the value of $\Delta\gamma_{MM}$ approximated without nonreciprocal effects. After substituting derivatives of Ω into (20), we acquire

$$(\Delta\gamma l_N - \Delta\gamma_{MM} p)\sinh(\gamma_{MMo} p) = 0$$

With respect to pure imaginary $\Delta\gamma_{NR} \approx j\Delta\beta_{NR}$ in lossless approximation, the equation above gives nonreciprocity for the periodic structure

$$\Delta\beta_{MM} \approx -j\Delta\gamma_{MM} \approx \Delta\beta_{NR} l_N / p \tag{21}$$

Equation (21) states the linear dependence of the nonreciprocity on the longitudinal fraction of nonreciprocal section in the unit cell. The estimation of the nonreciprocity as a function of the frequency is plotted for the validity with a magenta dash-dot line in Fig. 6(a).

4.4 Numerical Simulation

In Fig. 6(c), S-parameters of the metamaterial are obtained for a finite number of unit cells n_{cells} from $F_{Cell}^{n_{cells}}$. Figure 6 also includes the FEM numerical simulation results by ANSYS HFSS™ ver.13 for comparison. The simulated phase shift was converted for convenience into dispersion diagram in Fig. 6(a). The calculations by the proposed approach are in good agreement with the numerical simulation. Visible discrepancy below the cutoff is caused by the fact that FEM simulation is carried out for finite number of cells and in the cutoff region, so simulation errors increase significantly due to the small amplitude of transmission coefficients for the damping mode. For that reason, the simulation below the cutoff was made for 8 unit cells, while other simulations are processed for 30 unit cells. Small nonreciprocity found in the magnitude of S_{21} and S_{12} is about 1 dB, and originates from nonreciprocity of attenuation constant, as confirmed in Fig. 4. It is caused by small dissipation factor ΔH used in the simulation. The proposed approach has not taken into account the radiation losses that make up about a half of total losses around cutoff in the example. We believe that discrepancy between analyzed and simulated Bloch impedances in Fig. 6(b) can be explained by the effective electromagnetic width of the structure, which is larger than w and can vary depending on the stub parameters and period p.

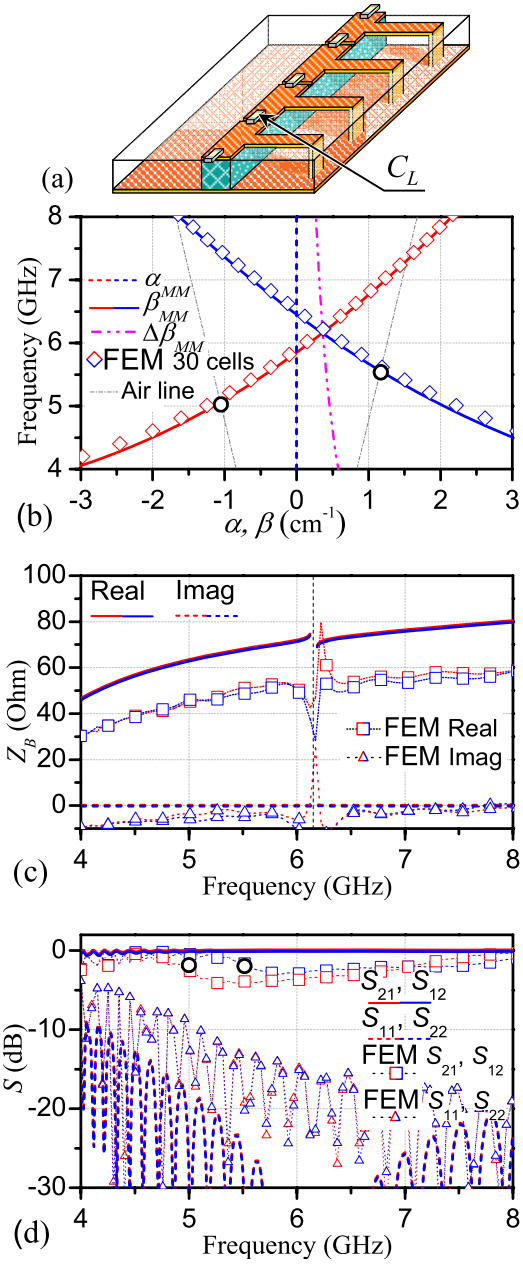

Fig. 7 Comparison of the proposed approach with numerical simulation of nonreciprocal CHRL metamaterial. (a) Schematic appearance of the metamaterial transmission line. (b) Dispersion diagram. (c) Characteristic Bloch impedance. (d) S-parameters.

5. Analysis of CRLH Structure

The proposed ε-negative structure can be converted to CRLH transmission line by means of series capacitors introduced in the circuit, as shown in Fig. 7(a). By providing a capacitance of certain value, we can create a μ-negative frequency band with the same cutoff frequency as in the ε-negative structure, thus supporting gapless propagation below the cutoff. The series capacitance C_L is introduced in the unit cell in the form of ABCD matrices F_{2CL} of double capacitances $2C_L$ by $F_{Cell} = F_{2CL}F_{RS}F_{NRS}F_{RS}F_{2CL}$. Figures 7(b), (c), (d) illustrate the dispersion, Bloch impedance and S-parameters acquired by using (13) and (15) in comparison with the results of FEM simulation. Configuration parameters are the same as in previous section. The capacitance has a value $C_L = 0.3$ pF in the proposed model and simulation. Good agreement with FEM simulation was achieved. In Fig. 7(d), the discrepancy above 5–5.5 GHz for S_{21} and S_{12}, respectively, is related to the radiation losses that are not taken into account in the proposed approach. Lower radiation band bounds are marked with round marks in Fig. 7(d) and exactly correspond to intersection of dispersion diagram with air lines, as shown in Fig. 7(b). The discrepancy in Bloch impedance in Fig. 7(c) has the same nature as discussed in Sect. 4.2.

6. Experimental Investigation

Although it is not the first time that the phase-constant nonreciprocal metamaterial is being presented in experimental work [12], [16], the main aim of this subsection is to prove that the model proposed in this paper gives a good explanation to measured nonreciprocal transmission coefficients.

The ε-negative and CRLH metamaterial structures were constructed. The designed operational frequencies of the metamaterials and the frequency range of experiment were chosen to be considerably higher than ferromagnetic resonance. The structures were designed using the proposed approach to provide a considerable magnitude of phase-constant nonreciprocity of approximately 0.3–0.4 cm^{-1} near the cutoff.

The photos of the prototype transmission lines are shown in Fig. 8. Both structures were fabricated by microstrip technology. First, the 45 mm-length YIG ferrite rod of 0.8 mm × 0.8 mm in cross-section was fixed with dielectric glue on the brass ground plate between two SMA-microstrip connectors. A copper strip of 45 mm × 0.8 mm was attached to the top face of the ferrite rod, thus forming a ferrite-embedded microstrip line. A set of microstrip shunt stubs was produced with a period $p = 4$ mm on the 0.8 mm-thick Rexolite^{TM} 2200 substrate and affixed to the microstrip line. For the ε-negative structure in Fig. 8(a), the stub length was 1.86 mm, and for CRLH structure in Fig. 8(b), the stub length was 1.7 mm. Series capacitors with a capacitance C_L = 0.2 pF were inserted in the gaps between unit cells of the CRLH structure. The assemblies were placed into external saturating dc magnetic field $\mu_o H_{ext} = 100$ mT, normal to the microstrip line. The circuit was connected to Agilent^{TM} PNA series network analyzer where complex S-parameters and phase shifts in both directions were measured in the frequency range of 5–9 GHz.

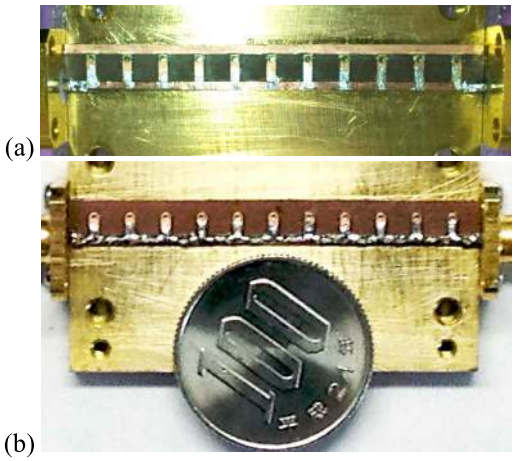

Fig. 8 Experimental model of the metamaterial TL. (a) ε-negative structure, (b) CRLH structure.

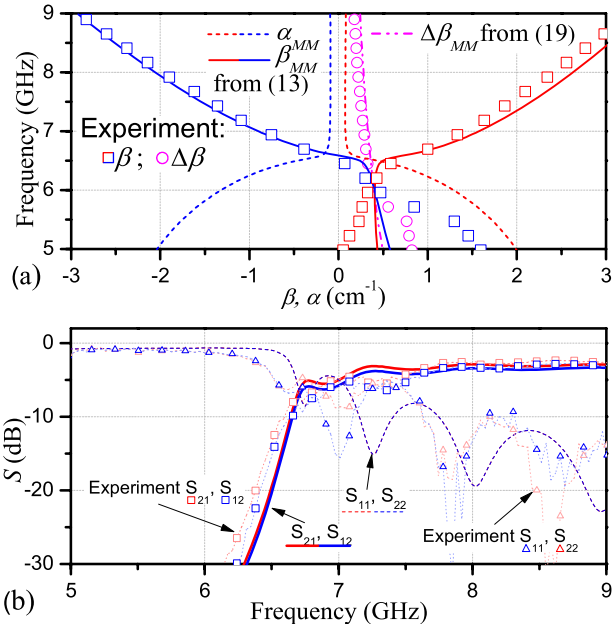

Fig. 9 Comparison of the proposed model with experiment for the ε-negative metamaterial. (a) Dispersion diagram. (b) S−parameters. Solid and dashed lines are for the proposed approach, figure marks are for experimental data.

The phase shift data were converted for convenience into dispersion diagram in Fig. 9(a) and Fig. 10(a). The amplitude responses for both structures are presented in Fig. 9(b) and Fig. 10(b). In both figures, results of our modeling are presented with solid and dashed lines, experimental results are presented with figure marks.

The analytic dispersion diagram and S-parameters profile were calculated by taking into account the magnetic dis-

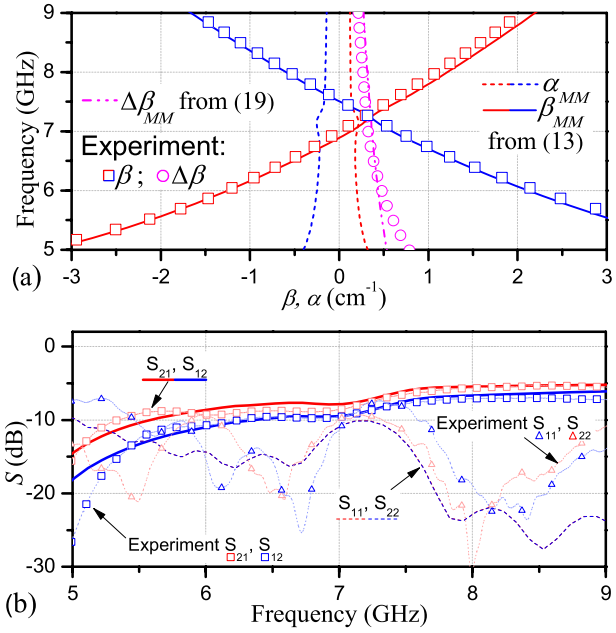

Fig. 10 Comparison of the proposed model with experiment for the CRLH metamaterial. (a) Dispersion diagram. (b) S-parameters. Solid and dashed lines are for the proposed approach, figure marks are for experimental data.

sipation with factor $\mu_o \Delta H = 4\,\mathrm{mT}$ for polycrystalline YIG and finite resistive part of boundary impedances. The results show good agreement with the experimental data and calculations within the guided wave frequency region. The metamaterials exhibits nonreciprocity in the phase constant of $0.35\,\mathrm{cm}^{-1}$ for ε-negative structure, and $0.31\,\mathrm{cm}^{-1}$ for CRLH structure, that is close to the expected value and the discrepancy can be explained by imperfect assembly quality. Larger discrepancy of phase constant below the cutoff in Fig. 9(a) originates from parasitic resonance notches at 5.5 GHz that could be seen only below a level of −60 dB. In Fig. 10, a small band-gap can be identified at 7.25 GHz that is caused by deviation of C_L from the projected value. This deviation was taken into account in our model when preparing Fig. 9. The port impedance mismatch caused by the band-gap, resulting in increased insertion loss below 7 GHz was also taken into account.

Both Fig. 9 and Fig. 10 show good agreement between the present model, and the experiment, especially in the guided wave region. According to our further analysis, small nonreciprocity of the magnitude of transmission coefficients, found in Fig. 10(b), could be reduced by the use of low-loss ferrites.

7. Conclusions

The proposed approach allowed estimating propagation characteristics of the nonreciprocal metamaterials composed of the normally magnetized ferrite-embedded microstrip line periodically loaded with stubs demonstrating a good precision. The present approach described not only ε-negative characteristics below the cutoff but also the nonreciprocity in phase characteristics of the metamaterial. The analysis carried out also revealed and explained a number of methods of control over nonreciprocity that give certain freedom in design of nonreciprocal transmission line based metamaterials.

It was demonstrated that the proposed approach is well applicable to the analysis of both nonreciprocal CRLH and ε-negative metamaterials without significant changes in the model.

References

[1] C. Caloz and T. Itoh, Electromagnetic Metamaterials: Transmission Line Theory and Microwave Application, John Wiley & Sons, 2006.
[2] G. Eleftheriades and K. Balmain, Negative refraction metamaterials, John Wiley & Sons, 2005.
[3] A. Lai, C. Caloz, and T. Itoh, "Composite right/left-handed transmission line metamaterials," IEEE Microw. Mag., vol.5, no.3, pp.34–50, Sept. 2004.
[4] G. Elefteriades, A. Iyer, and P. Kremer, "Planar negative refractive index media using planar L-C loaded transmission line," IEEE Trans. Microw. Theory Tech., vol.50, no.12, 2702–2712, 2002.
[5] T. Ueda and M. Tsutsumi, "Nonreciprocal left-handed transmission characteristics of microstrip lines on the ferrite substrate," IET Proc. Microw. Antennas Propag., vol.1, no.2, pp.349–354, April 2007.
[6] T. Ueda and M. Tsutsumi, "Left-handed transmission characteristics of ferrite microstrip lines without series capacitive load," IEICE Trans. Electron., vol.E89-C, no.9, pp.1318–1323, Sept. 2006.
[7] M. Abdalla and Z. Hu, "On the study of nonreciprocal left handed coplanar waveguide over ferrite substrate with only shunt inductive load," Microw. Opt. Tech. Lett., vol.49, no.11, pp.2810–2814, 2007.
[8] T. Kodera and C. Caloz, "Uniform ferrite-loaded open waveguide structure with CRLH response and its application to a novel backfire-to-endfire leaky-wave antenna," IEEE Trans. Microw. Theory Tech., vol.57, no.4, pp.784–795, April 2009.
[9] T. Ueda, K. Horikawa, M. Akiyama, and M. Tsutsumi, "Nonreciprocal phase-shift composite right/left handed transmission lines and their application to leaky wave antennas," IEEE Trans. Antennas Propag., vol.57, no.7, pp.1995–2005, July 2009.
[10] T. Ueda, "Transmission line microwave apparatus including at least one non-reciprocal transmission line part between two parts," U.S. Patent US 8, 294, 538 B2, Oct. 23, 2012.
[11] K. Horikawa, T. Ueda, and M. Akiyama, "Influence of reflected waves at a terminal of nonreciprocal phase-shift CRLH transmission lines on the leaky wave radiation," Proc. 2009 Asia-Pacific Microw. Conf., pp.151–154, Dec. 2009.
[12] T. Ueda and H. Kishimoto, "Pseudo-traveling wave resonator based on nonreciprocal phase-shift composite right/left handed transmission lines," 2010 IEEE MTT-S Int. Microw. Symp. Digest, pp.41–44, May 2010.
[13] T. Ueda, S. Yamamoto, Y. Kado, and T. Itoh, "Pseudo-traveling wave resonator with magnetically tunable phase gradient of fields and its applications to beam steering antennas," IEEE Trans. Microw. Theory Tech., vol.60, no.10, pp.3043–3054, Oct. 2012.
[14] A. Sanada, C. Caloz, and T. Itoh, "Zeroth-order resonance in composite right/left handed transmission line resonators," Proc. 2003 Asia-Pacific Microw. Conf., pp.1588–1592, Nov. 2003.
[15] M. Abdalla and Z. Hu, "Design and analysis of tunable left handed zeroth-order resonator on ferrite substrate," IEEE Trans. Magn., vol.44, pp.3095–3098, Nov. 2008.
[16] T. Ueda, S. Yamamoto, and Y. Kado, "Beam-scanning traveling-wave- resonator antenna based on nonreciprocal phase-shift CRLH transmission lines," 2011 IEEE Int. Symp. Antennas Propag. Proc., pp.1058–1061, July 2011.

[17] R.E. Collin, Foundations for Microwave Engineering, 2nd ed., IEEE Press-Wiley, 2001
[18] J. Weiss, "Reciprocal and nonreciprocal microstrip periodic networks," Report on Project ARPA Order no.498, July 1967.
[19] A. Porokhnyuk, T. Ueda, Y. Kado, and T. Itoh, "Mode analysis of nonreciprocal metamaterials using a combination of field theory and transmission line model," 2012 IEEE MTT-S Int. Microw. Symp. Digest, WE4J-5, pp.1–3, June 2012.
[20] M.E. Hines, "Reciprocal and nonreciprocal modes of propagation in ferrite striopline and microstip devices," IEEE Trans. Microw. Theory Tech., vol.MTT-19, no.5, pp.442–451, May 1971.
[21] T. Ueda and M. Akiyama, "Nonreciprocal phase-shift composite right/left handed transmission lines using ferrite-rod-embedded substrate," IEEE Trans. Magn., vol.45, no.10, pp.4203–4206, Oct. 2009.
[22] H. Kishimoto, T. Ueda, and Y. Kado, "Experimental demonstration of nonreciprocal phase-shift composite right/left handed transmission lines using a ferrite-rod-embedded substrate," IEEE Trans. Magn., vol.47, no.10, pp.3724–3727, Oct. 2011.
[23] T. Ueda, J. Fukuda, Y. Kado, and T. Itoh, "Nonreciprocal phase-shift CRLH transmission lines using geometrical asymmetry with periodically inserted double shunt stubs," 42nd Eur. Microw. Conf., pp.570–573, Oct. 2012.
[24] E.O. Hammerstad, "Equations for microstrip circuit design," Proc. 5th Eur. Microw. Conf., pp.268–72, Sept. 1975.
[25] B. Lax and K.J. Button, Microwave Ferrites and Ferrimagnetics, McGraw-Hill, New York, 1962.

Andrey Porokhnyuk received the M.E. degree in Electronics in the field of spin-wave technology from St. Petersburg State Electrotechnical University "LETI" in 2003. At present time, he is accomplishing the Ph.D. program at Kyoto Institute of Technology studying the metamaterial technology.

Tetsuya Ueda received the B.E., M.E., and Ph.D. degrees in communication engineering from Osaka University, Osaka, Japan, in 1992, 1994, and 1997, respectively. Since 1997, he has been with the Department of Electronics, Kyoto Institute of Technology, Kyoto, Japan, where he is currently an Associate Professor. From 2005 to 2006, he was a Visiting Scholar with the Department of Electrical Engineering, University of California, Los Angeles (UCLA). His current research interests include metamaterials and their applications. Dr. Ueda was the recipient of the 1999 IEICE Young Engineer Award and the 2008 IEEE MTT-S Japan Chapter Young Engineer Award. He is a Senior Member of the IEEE.

Yuichi Kado received M.S. and Ph.D. degrees in electronics from Tohoku University, Miyagi, Japan, in 1983 and 1998, respectively. In 1983 he joined the Electrical Communication Laboratories of Nippon Telegraph and Telephone Public Corporation (now NTT), Kanagawa, Japan, where he was engaged in research on SOI structure formation by hetero-epitaxial growth. From 1989 to 1998 he worked on the development of fully depleted CMOS/SIMOX LSIs and ultra-low-power CMOS circuits. From 1999 he was engaged in R&D on compact network appliances using ultralow-power CMOS circuit technologies for ubiquitous communications. He led research and development projects on ultra-low-power network appliances, sub-terahertz-wave wireless communication, and intra-body communication as a director of Smart Devices Laboratory at NTT Microsystem Integration Laboratories (2003–2010). In July 2010, he joined the Department of Electronics, Kyoto Institute of Technology, Kyoto, Japan. He has been the recipient of awards including the 2009 Nikkei BP Technology Award, the 2009 Radiowave Achievement Award presented by the ARIB, and the 2011 Session's Best Paper Award presented by the IIIS. He is a member of IEEE.

Tatsuo Itoh received the Ph.D. Degree in Electrical Engineering from the University of Illinois, Urbana in 1969. After working for University of Illinois, SRI and University of Kentucky, he joined the faculty at The University of Texas at Austin in 1978, where he became a Professor of Electrical Engineering in 1981. In September 1983, he was selected to hold the Hayden Head Centennial Professorship of Engineering at The University of Texas. In January 1991, he joined the University of California, Los Angeles as Professor of Electrical Engineering and holder of the TRW Endowed Chair in Microwave and Millimeter Wave Electronics (currently Northrop Grumman Endowed Chair). He received a number of awards including IEEE Third Millennium Medal in 2000, and IEEE MTT Distinguished Educator Award in 2000. He was elected to a member of National Academy of Engineering in 2003. In 2011, he received Microwave Career Award from IEEE MTT Society. Dr. Itoh is a Fellow of the IEEE and Commissions B and D of USNC/URSI. He served as the Editor of IEEE Transactions on Microwave Theory and Techniques for 1983–1985. He was President of the Microwave Theory and Techniques Society in 1990. He was the Editor-in-Chief of IEEE Microwave and Guided Wave Letters from 1991 through 1994. He was elected as an Honorary Life Member of MTT Society in 1994. He was the Chairman of Commission D of International URSI for 1993–1996, and the Chairman of Commission D of International URSI for 1993–1996. He serves on advisory boards and committees of a number of organizations. He served as Distinguished Microwave Lecturer on Microwave Applications of Metamaterial Structures of IEEE MTT-S for 2004–2006. He has 400 journal publications, 840 refereed conference presentations and has written 48 books/book chapters in the area of microwaves, millimeter-waves, antennas and numerical electromagnetics. He generated 75 Ph.D. students.